Comparison of Ellison and Thorpe scales from Eulerian ocean temperature observations.

Andrea Cimatoribus* and Hans van Haren

Royal Netherlands Institute for Sea Research, Texel, The Netherlands

Louis Gostiaux

Laboratoire de Mécanique des Fluides et d'Acoustique, CNRS/Université de Lyon, Lyon, France

The spatial and temporal distribution of turbulence dissipation rate in the ocean is not well known. In the ocean, turbulence dissipation rate is measured either by means of microstructure shear measurements, seldom performed in the open and deep ocean, or by means of adiabatically reordering vertical profiles of density. The latter technique leads to the estimation of the typical overturn size, the Thorpe scale, which can be used to estimate average turbulence dissipation rate by using empirical relations linking the Thorpe scale to the Ozmidov scale of turbulence. In both cases, the turbulence dissipation rate is estimated using single vertical profiles from shipborne instrumentation, having limited time resolution.

We present here an alternative method to estimate the typical overturn size by measuring the Ellison length scale using frequency spectra of temperature just beyond the internal wave band, measured by moored instruments. We apply the method to high resolution temperature data from three moorings deployed at different locations around the Josephine sea mount (North Eastern Atlantic Ocean). It is shown that the variance of the temperature time series at the higher end of the internal wave frequency band and above is well correlated with the overturn size. The method is based on a time frequency decomposition using the "maximum overlap discrete wavelet transform". This method can be a viable alternative for indirectly estimating turbulence dissipation rate from moored instruments in the ocean if time resolution is sufficiently high.

A major result is the indication that fine structure contaminated temperature measurements can in fact provide reliable information on turbulence intensity.

arXiv:1402.6958v1 [physics.flu-dyn] 27 Feb 2014

* Andrea.Cimatoribus@nioz.nl

I. INTRODUCTION

Turbulence dissipation rate is a key quantity in a turbulent flow, but its value, temporal and geographical distribution are poorly known in the ocean. Turbulence dissipation rate is defined as $\epsilon = \nu\overline{\left(\frac{\partial u_i'}{\partial x_i}\right)^2}$, where ν is the kinematic viscosity, $u_i' = u_i - \overline{u}_i$ is the component of the velocity fluctuation along the x_i direction, summation over repeated indices is assumed and the overbar implies an appropriate time, space or ensemble average (see, e.g., Frisch, 1996).

Direct estimation of ϵ in the ocean interior is not routinely performed as it implies the measurement of velocity shear at the millimetre scale where most of the dissipation actually takes place (see for instance the shipborne microstructure measurements of Gregg, 1987; Oakey, 1982; Polzin *et al.*, 1997). Resolving the microstructure shear in the deep ocean is impractical due to various reasons ranging from the cost of deep-ocean shear profilers to the challenge represented by the interpretation of the raw data due to, e.g., vibrations of the instrument (for a review on the instrumentation, see, e.g. Lueck *et al.*, 2002).

Measurements of shipborne CTD (conductivity, temperature, depth), or temperature and depth alone, are generally less expensive. Consequently, an indirect approach is often followed enabling to estimate the average turbulence dissipation rate from the characteristic size of the overturns in a stratified water column (Dillon, 1982; Gargett, 1989; Gregg, 1987; Itsweire, 1984; Thorpe, 1977). In particular, ϵ can be estimated by measuring the scale of largest overturns unaffected by stratification for a given turbulence level and stratification, the Ozmidov scale $L_O = (\epsilon/N^3)^{\frac{1}{2}}$, with N the buoyancy frequency. The Ozmidov scale can be compared to an objective measure of the overturns size in the water column. A common choice is the Thorpe scale (L_T), defined as the root mean square of the displacement needed to adiabatically reorder a profile containing density inversions due to overturns (Thorpe, 1977). Dillon (1982) estimated the ratio L_O/L_T to be approximately 0.8; this linear relationship has been discussed in several papers, which confirmed it for fully developed turbulence (e.g., Itsweire *et al.*, 1993). Other works suggest that the ratio may not be constant (e.g. Mater *et al.*, 2013; Smyth and Moum, 2000; Smyth *et al.*, 2001). Following Dillon (1982), turbulence dissipation rate is estimated by the formula:

$$\epsilon_{L_T} = 0.64 \cdot L_T^2 N^3, \tag{1}$$

where the constant is the one measured by Dillon (1982) and confirmed by Crawford (1986), the subscript of ϵ is a reminder of the method used for the estimation. If only temperature is measured, as often done in practice, a key requirement for applying (1) is that a tight temperature–density relationship is found, so that temperature is a good proxy of density. Both estimation methods of the turbulence dissipation rate, direct and indirect, are in most cases used on isolated measurements, from either free-falling, free-raising or lowered instruments.

Here, we develop an alternative method to estimate L_T, and thus the turbulence dissipation rate, using frequency spectra of temperature at fixed depth, measured by moored instruments. These frequency spectra are used to estimate the Ellison scale (defined in section II.A) which we relate to the Thorpe scale. We will show that the part of the temperature frequency spectrum immediately beyond the internal wave band is the one best correlated with the turbulence dissipation rate. This part of the spectrum is in fact the one most affected by fine structure contamination, i.e. spectral contamination due to the advection of sharp gradients (Gostiaux and van Haren, 2012; Phillips, 1971). Comparisons between the Thorpe scale and the Ellison scale from laboratory experiments and numerical simulations are available in the literature, to our knowledge at least in Itsweire (1984), Gargett (1988), Itsweire *et al.* (1993), Smyth and Moum (2000) and Mater *et al.* (2013). We are, however, unaware of such a comparison in the ocean, and of a comparison which analyses in detail the role of the time scales involved; these are the main motivations for this work.

In this context, the datasets obtained using NIOZ high sampling rate thermistors (e.g., van Haren and Gostiaux, 2012) provide with a unique opportunity to study the temporal variability of turbulence in the ocean. These thermistors, deployed in a mooring, can measure temperature continuously and independently for up to two years, with a temporal resolution of 1 Hz and a vertical resolution set by the thermistor separation along the mooring line, usually about 1 m. A growing set of measurements has been collected in various locations, ranging from tidally dominated shores (van Haren *et al.*, 2012) to seamounts (van Haren and Gostiaux, 2012), to the deep and open ocean (van Haren and Gostiaux, 2009, 2011). We will consider here three data sets, which combine high temporal resolution with a reliable estimation of the vertical density profile.

This article is structured as follows: in section II.A we outline the theoretical grounds of the data analysis. In section II.B we briefly describe the data sets used. In section II.C we describe the data analysis procedure. Results are presented in section III and discussed in section IV. A brief summary of the main points follows in section V.

II. METHODS

A. Theory

We write the time series obtained from the Eulerian measurement of potential temperature at some fixed depth $\hat{z}$ as $\theta_{\hat{z}}(t)$. We will consider potential temperature equivalently to potential density, an assumption justified for the data sets used (see section II.B). We assume that, on a sufficiently short time scale τ, $\theta_{\hat{z}}(t)$ can be described by a "rigid" vertical temperature profile advected in time by the vertical displacement $\zeta(t)$. Under this assumption, we write the Eulerian time-dependent temperature anomaly as:

$$\theta'_{\hat{z}}(t) = \theta(\hat{z} + \zeta(t)) - \theta(\hat{z}),$$

where θ (without subscript, function of the vertical coordinate) is the temperature profile averaged over a time τ (θ is thus independent of time over τ). The Fourier transform of $\theta'_{\hat{z}}(t)$ is defined as:

$$\mathcal{F}\left[\theta'_{\hat{z}}\right](\omega) = \int_{-\infty}^{+\infty} \theta'_{\hat{z}}(t) \mathrm{e}^{-2\pi i \omega t}\, \mathrm{d}t$$

where ω is the frequency.

We consider a Taylor expansion for $\theta'_{\hat{z}}(t)$ in $\zeta(t)$:

$$\theta'_{\hat{z}}(t) = \left.\frac{\mathrm{d}\theta}{\mathrm{d}z}\right|_{\hat{z}} \zeta(t) + \mathcal{O}(\zeta^2). \tag{2}$$

Keeping the first-order terms, we can write:

$$\mathcal{F}\left[\theta'_{\hat{z}}\right](\omega) \approx \left.\frac{\mathrm{d}\theta}{\mathrm{d}z}\right|_{\hat{z}} \mathcal{F}\left[\zeta\right](\omega) = -\frac{1}{g\alpha} N_\theta^2\, \mathcal{F}\left[\zeta\right](\omega),$$

where we introduced the notation $\left.\frac{\mathrm{d}\theta}{\mathrm{d}z}\right|_{\hat{z}} = -\frac{N_\theta^2}{g\alpha}$, with g the acceleration of gravity and α the thermal expansion coefficient. We stress that N_θ, the buoyancy frequency computed from the potential temperature profile, is evaluated at the fixed depth $\hat{z}$ and computed from the temperature profile averaged over τ.

We thus conclude that the power spectrum $\mathcal{S}\left[\theta'_{\hat{z}}\right](\omega) = \left|\mathcal{F}\left[\theta'_{\hat{z}}\right](\omega)\right|^2$ is given by:

$$\mathcal{S}\left[\theta'_{\hat{z}}\right](\omega) = \frac{1}{g^2\alpha^2}\, N_\theta^4\, \mathcal{S}\left[\zeta\right](\omega). \tag{3}$$

Equation (3) states that, for frequencies higher than τ^{-1}, the spectrum of displacement and the spectrum of temperature are linearly related. The validity of (3) is limited to frequencies higher than τ^{-1} since on longer time scales diffusion and horizontal advection will change the vertical temperature profile; for lower frequencies the assumption of rigid vertical advection of the temperature profile does not hold[1].

We now consider the Ellison length scale, defined as in, e.g., (Mater *et al.*, 2013):

$$L_E = \frac{\overline{\rho'^2}^{1/2}}{|\partial\rho/\partial z|},$$

where ρ' is the perturbation density around a reference density profile ρ to be specified. If the reference vertical profile is the adiabatically reordered (Thorpe) one then L_E is, at first order, equal to the Thorpe scale (Smyth *et al.*, 2001). In this context, we follow a slightly different approach, and we use the linear expansion in (2), defining L_E as:

$$L_E = \frac{\overline{\left(\theta'_{\hat{z}}\right)^2}^{1/2}}{\mathrm{d}\theta/\mathrm{d}z|_{\hat{z}}} = \frac{\sigma_{\theta_{\hat{z}}}}{\mathrm{d}\theta/\mathrm{d}z|_{\hat{z}}} \approx \sigma_\zeta, \tag{4}$$

with σ_ζ and $\sigma_{\theta_{\hat{z}}}$ the root mean square of ζ and $\theta'_{\hat{z}}$ respectively. In (4) the overbar is understood as averaging over the time τ discussed above. The reference profile in (4) is thus not the Thorpe reordered one, but a time average

[1] This does not imply that the vertical temperature profile is not correlated with itself for times longer than τ. Autocorrelation is present at all time scales, but diffusion and advection invalidate the linear relationship of equation (3).

one. We will show using observational data that L_E from this definition is a good approximation of the Thorpe scale. Equation (4) suggests to use (3) for estimating L_E^2, since $\int \mathcal{S}[\zeta]\mathrm{d}\omega \equiv \sigma_\zeta^2$ by Parseval's theorem. The advantage of this approach is that we estimate L_E by using information only from a neighbourhood of $\hat{z}$, without reordering the whole vertical profile as is the case for computing Thorpe scales. Furthermore, the introduction of a frequency spectrum, i.e. of a frequency decomposition of the variance of ζ, enables us to compare L_E to L_T without violating the condition of rigid advection only for times shorter than τ. We can at this point rephrase the aim of this work as finding the relationship between the Thorpe scale and the Ellison scale as defined by (4), keeping in mind that we can estimate L_E even if temperature is not a good proxy for density.

Combining (4) and (3) we finally obtain our estimate:

$$\sigma_{\theta_{\hat{z}}}^2 \approx \frac{1}{g^2\alpha^2} N_\theta^4 L_E^2, \tag{5}$$

which we will use to measure L_E in different frequency bands. Furthermore, using (5) with (1), we obtain:

$$\sigma_{\theta_{\hat{z}}}^2 \approx \frac{1.5625}{g^2\alpha^2} N_\theta^4 N^{-3} \epsilon_{L_E}, \tag{6}$$

which provides a different estimate of ϵ, based on the variance of temperature (the subscript of ϵ is a reminder of this), to be compared with the one obtained from Thorpe scales. In (6), we distinguish between N_θ, the local temperature stratification which the thermistors always provide, and N, the physically relevant background buoyancy frequency. The two can be equal if temperature is a good proxy for density, but will differ if salinity compensation or other effects prevent a reliable reconstruction of the vertical density profile. In these cases, the background N has to be recovered from other measurements, which will usually be profiles from shipborne CTD measurements. In this work, we will not consider in detail this latter case.

B. Data

The three data sets used in this work come from three different moorings, deployed from spring to early fall 2013 in the Atlantic Ocean above the slopes of Seamount Josephine (details of the moorings are given in Table I). Each of the moorings had more than one hundred "NIOZ4" thermistors (an evolved version of the ones described in Hans van Haren *et al.*, 2009) taped on a nylon-coated steel cable, at intervals of 0.7 m (mooring 1) or 1.0 m (moorings 2 and 3). The thermistors sampled temperature at a rate of 1 Hz with a precision higher than 1 mK. The moorings were attached to a ballast weight at the bottom, and to an elliptical buoy at the top. The high tension on the string, due to the high net buoyancy (approximately 400 kg) guarantees that the string behaves as a rigid rod, and that the mooring excursion both in the vertical and in the horizontal directions are small, as checked in similar previous moorings (van Haren and Gostiaux, 2012). All the thermistors in mooring 1 performed satisfactorily for the whole deployment, with a noise level of approximately $5 \cdot 10^{-5\circ}$ C. On the other hand, in mooring 2, 7 thermistors out of 140 provide no data due to battery or electronic failure. In mooring 3, 2 thermistors out of 170 have no data, and 2 more have missing data after approximately the first 50 days due to battery failure. One more thermistor in mooring 3 is not used, despite recording data during the whole deployment, due to a problem in the calibration. Finally, one thermistor in mooring 3 has a higher noise level than the others, in the order of $10^{-3\circ}$ C due to the use of a wrong setting, and is for this reason excluded from the analysis. Overall, signal-to-noise ratio in moorings 2 and 3 is smaller than in mooring 1, mainly due to the smaller (approximately 10 times) temperature variations at the greater depth of these moorings. This limits the accuracy of our Thorpe scale estimates from moorings 2 and 3, as well as the accurate estimation of temperature variance. We thus focus our analyses on mooring 1, and consider the other two moorings for comparison and for assessment of the skill of the technique developed for mooring 1 in sub-optimal conditions.

As mentioned in section I, a key requirement for reliably estimating Thorpe scales and turbulence dissipation rate from temperature measurements is a tight temperature-salinity relationship. On top of this, a linear density–temperature relationship in the measured temperature range further ensures that temperature is a good proxy of density. In order to check if these assumptions are valid for the data considered here, two CTD surveys were performed. The first one was performed after the recovery of mooring 1, sampling the water column approximately between 2000 m and 10 m above the bottom while the ship was moving at less than 1 knot towards the deployment location of moorings 2 and 3. The results of this survey are summarised in figure 1-a, which shows potential density anomaly as a function of temperature for 2 m binned data between 2000 m and 2500 m (approximately the bottom depth). The depth range is chosen in order to include approximately the same temperature range as the one recorded at mooring 1 ($3.5 - 4.5^\circ$ C). The data comes from the first six downward casts of the CTD, the ones closer to mooring

1. Temperature from mooring 1 is higher by approximately 0.3° C during the last 20 days of the record than in the rest of the data set. This suggests that warm water is being advected to the mooring location, possibly due to the passage of a vortex or a front. As a consequence, this first CTD survey, performed during this warm phase, sampled warmer water than the thermistor string average at the same depth. Furthermore, while moving away from mooring 1, slightly different water masses were found in the higher temperature range (close to 2000 m depth). This shows up in the bottom right part of figure 1-a. Despite this, density–temperature relationship is overall rather tight, and a linear fit of the data, shown in the figure, gives a coefficient of determination R^2 of 0.997.

To better assess the linearity of the density–temperature relation, a more extensive survey was performed after the recovery of moorings 2 and 3. The survey included 8 casts of the column below 2500 m in a square region of side approximately 1 km centred at the mooring location, and 9 more casts over the whole water column, along two perpendicular transects of length approximately 20 km centred at the mooring location. The results of this second survey are collected in figure 1-b, showing potential density anomaly as a function of temperature for 2 m binned data between 2500 m and 3000 m from all the downward CTD casts. The data, spanning a broader temperature range than the one recorded at moorings 2 and 3, confirm the results of the first survey. A linear fit of the data gives an R^2 of 0.998, and temperature can be considered a reliable proxy for density. The larger spread of the data in panel b is partly due to considering all the casts together, and partly an artefact of the smaller temperature range plotted. If taken separately, each profile has a tight linear relationship (not shown).

C. Data processing

The data from the three different moorings is processed following the same procedure. Calibration is applied to the raw data and the drift in the response of the thermistor electronics, visible over periods longer than a couple of weeks, is compensated for.

1. Thorpe scale analysis

The full data from the moorings, at a 1 Hz sampling rate, is low-pass filtered and subsampled to a time step of 25 s using a non-overlapping moving average, for reasons of computational efficiency. The results are not sensitive to this subsampling, as was discussed first in van Haren and Gostiaux (2012) and confirmed on subsets of the data here. Missing data from moorings 2 and 3 (see section II.B) are linearly interpolated using data from the two thermistors directly above and below. Temperature is, at this point, transformed to potential temperature by using a constant thermal expansion coefficient; the correction is, however, minimal. The temperature profile at each time step is reordered to obtain the stably stratified reference profile, and to obtain an estimate of the Thorpe scale as the root mean square displacement of water parcels in this process. For further discussion of the computation of Thorpe scales in a comparable data set, see van Haren and Gostiaux (2012).

The probability density function of the Thorpe scales thus obtained is shown in figure 2-a for mooring 1. A typical size of the overturns is 10 m, and we note that while the vertical resolution (0.7 m for mooring 1) is sufficient to resolve the left tail of the distribution, the mooring length is imposing a cutoff to the right tail, i.e. overturns larger than the mooring are present. We thus have to be careful when comparing the largest values of L_T to L_E, as only the former is limited by the mooring length. This issue is not relevant at moorings 2 (figure 2-c) and 3 (not shown), for a combination of smaller overturns (typical size approximately 1/2 the one at mooring 1) and the use of longer moorings (see Table I).

By using the reordered temperature profile, the buoyancy frequency can further be estimated at each time step, and ϵ_{L_T} can thus be computed using (1). Both L_T and ϵ_{L_T} are a function of time alone, since L_T is the root mean square of displacement of each vertical temperature profile, and the column average of N is used (values at the top and bottom thermistors excluded).

The probability density function of the buoyancy frequency is shown in figure 2-b for mooring 1. The mean values of N are of order $10^{-3}\,\mathrm{s}^{-1}$ at mooring 1, first and 99th percentiles of the distribution are $N_1 \approx 10^{-3.7}\,\mathrm{s}^{-1}$ and $N_{99} \approx 10^{-2.3}\,\mathrm{s}^{-1}$. At moorings 2 and 3 the distributions of N have similar mean (approximately $10^{-3}\,\mathrm{s}^{-1}$) but smaller first and 99th percentiles ($N_1 \approx 10^{-3.9}\,\mathrm{s}^{-1}$ and $N_{99} \approx 10^{-2.5}\,\mathrm{s}^{-1}$) than at mooring 1. At moorings 2 and 3, N-distributions also have a broader peak than at mooring 1 (in particular mooring 2, see figure 2-d), but higher values of N are markedly less frequent, with a very short right tail of the distribution. All the statistics of N are computed excluding the values at the top and bottom thermistors, since the value of N is less reliable there, being computed using backward/forward differences instead of centred ones.

2. Wavelet analysis

As discussed in section II.A, the key assumption used for the comparison of L_E and L_T in ocean data is the rigid advection of the temperature profile, an assumption that holds only over a time scale τ to be determined. This was the reason behind the introduction of (3), which provides the basis for a frequency decomposition of the temperature variance, and for the identification of the frequency range that provides the best correlation between L_E and L_T. However, in order to make practical use of (5) and (6), and in particular in order to compare them with L_T and ϵ_{L_T} (both time dependent quantities), we must use a time–frequency decomposition of the temperature variance. One of the most commonly used time–frequency decompositions is the wavelet transform. In particular, we use here the "maximum overlap discrete wavelet transform" (MODWT) following the methods described in detail in Percival and Walden (2006). This wavelet method is mostly equivalent to the more commonly used "continuous wavelet transform" (see, e.g., Torrence and Compo, 1998, for a practical introduction to the continuous wavelet transform), but provides some computational advantages (Percival and Walden, 2006) over the continuous version, and was chosen for this reason.

Here, we shortly present the decomposition method following the summary given in Cornish *et al.* (2006). We consider the time series of one thermistor at a fixed depth $\theta_{\hat{z}}(t)$, which we denote here Θ_t for brevity. Given a finite length time series $\{\Theta_t\}$ with unit time step, sampled at times $t = 0, \ldots, (N-1)$, we want to decompose it in J_0 time scales $\tau_j = 2^{j-1}$, with $j = 1, \ldots, J_0$. At each level j, the decomposition formally implies the application of a wavelet filter ($\{h_{j,l}\}$, high-pass) and a scaling filter ($\{g_{j,l}\}$, low-pass), providing a set of wavelet ($\{W_{j,t}\}$) and scaling ($\{V_{j,t}\}$) coefficients respectively. The filters $\{h_{j,l}\}$ and $\{g_{j,l}\}$ can be computed at each level j by stretching the $j = 1$ base filters. Their length at each level is $L_j = (2^j - 1)(L-1) + 1$ with L the length of the base filter. In their simplest form, $\{h_{j,l}\}$ and $\{g_{j,l}\}$ perform, respectively, a running differentiation and running mean of the time series. Using "reflection boundary conditions" to reduce the impact of the time series being of finite length and non-periodic, a new time series is defined from the original one:

$$\{\widetilde{\Theta}_t\} = \begin{cases} \Theta_t & \text{for } t = 0, \ldots, N \\ \Theta_{2N-1-t} & \text{for } t = N, \ldots, 2N-1. \end{cases}$$

The wavelet and scaling coefficients are then defined for each j respectively as:

$$\begin{aligned} W_{j,t} &= \sum_{l=0}^{L_j-1} h_{j,l} \widetilde{\Theta}_{j,t-l \bmod 2N} \\ V_{j,t} &= \sum_{l=0}^{L_j-1} g_{j,l} \widetilde{\Theta}_{j,t-l \bmod 2N}, \end{aligned} \tag{7}$$

where $\{\widetilde{\Theta}_{1,t}\} = \{\widetilde{\Theta}_t\}$, $\{\widetilde{\Theta}_{j,t}\} = \{V_{j-1,t}\}$ for $j = 2, \ldots, J_0$, and mod represents the modulo operation. The MODWT coefficients have been circularly shifted in time in order to align them to the original time series as described in Percival and Walden (2006) (pag. 112). We want to stress that in practice boundary conditions are to a large extent irrelevant here, since we will consider short time scales compared to the time series length. Each wavelet coefficient set thus obtained nominally characterises the period range $[2^j, 2^{j+1})$ or, in other words, the time scale 2^{j-1}[2]. We stress that the correspondence between MODWT level and period range is imperfect since the MODWT decomposition, as any other filtering procedure, suffers from spectral leakage, i.e. leakage of power between nearby frequency bands. The wavelet coefficients set at each level has zero average; together with the J_0-level scaling coefficients set they conserve the time series "energy":

$$\|\mathbf{\Theta}\|^2 = \sum_{j=1}^{J_0} \|\mathbf{W}_j\|^2 + \|\mathbf{V}_{J_0}\|^2, \tag{8}$$

where $\|.\|$ indicates the Euclidean norm and the bold fonts denote vectors ($\mathbf{X} = \{X_t\}$). From (8) a scale decomposition of the variance is obtained:

$$\sigma^2_\Theta = \|\mathbf{\Theta}\|^2 - \overline{\mathbf{\Theta}}^2 = \frac{1}{N}\sum_{j=1}^{J_0} \|\mathbf{W}_j\|^2 + \frac{1}{N}\|\mathbf{V}_{J_0}\|^2 - \overline{\mathbf{\Theta}}^2, \tag{9}$$

---

[2] Intuitively, 2^{j-1} represents an "effective" Nyquist frequency for coefficients of level j.

where $\overline{\mathbf{\Theta}}$ is the mean value of $\{\Theta_t\}$. The time–frequency decomposition of the variance we were looking for, at time t and level j, is thus $W^2_{j,t}$, whose expected value is the variance at the time scale 2^{j-1}. Since $W^2_{j,t}$ is effectively a random process, rather than considering a single realisation of $W^2_{j,t}$ we will perform a non-overlapping running average of M realisations to increase the statistical significance of the variance estimate:

$$\left\langle W^2 \right\rangle^M_{j,t} = \frac{1}{M} \sum_{l=t-(M-1)/2}^{t+(M-1)/2} W^2_{j,l},$$

defined for times t multiple of M and for odd M. Finally, we consider the sum over $J \leq J_0$ levels:

$$\Sigma^M_{J,t} = \sum_{j=1}^{J} \left\langle W^2 \right\rangle^M_{j,t}, \tag{10}$$

which will be the key quantity used for computing L_E. $\Sigma^M_{J,t}$ represents the variance in the temperature time series at periods shorter than 2^{J+1}. After finding the value J maximising the correlation between L_E and L_T, the time scale τ is thus naturally identified with 2^{J+1}, since $\Sigma^M_{J,t}$ measures the variance in the time series if variations with periods longer than 2^{J+1} are removed. For further insight into the theoretical aspects of the MODWT, we refer to Percival and Walden (2006), in particular Chapters 5 and 8.

In order to apply the technique outlined so far on the time series from each thermistor, the full data are first low-pass filtered and subsampled to a time step of 7 s using a non overlapping moving average. The subsampling is necessary to reduce computing time, but we are confident that this is not affecting our results since the variance of the time series decays rapidly with increasing frequency, as discussed in detail in, e.g., van Haren and Gostiaux (2009). The subsampled time series can at this point be used to compute the wavelet and scaling coefficients defined in (7). The computation is performed using the pyramid algorithm described in detail in Percival and Walden (2006). The software used for this processing is freely available at the address https://sourceforge.net/projects/wmtsa/, and is mainly a python translation of the Matlab code available from the authors of Percival and Walden (2006) at the address http://faculty.washington.edu/dbp/wmtsa.html. The wavelet filter used is the "least asymmetric" one of length $L = 8$. The results presented here depend very weakly on the choice of the wavelet type; the length of the filter is chosen as a compromise between the temporal (short filter) and frequency (long filter) resolution, and also to minimise the influence of the boundaries for the longest time scales considered. The need to circularly shift the coefficients is a further reason to use the least asymmetric wavelets, since the phase shift introduced by them is known exactly a priori. The maximum level of the decomposition (J_0) is 13, which corresponds to a maximum period of 32 hours. The combination of a time step of 7 s with 13 decomposition levels guarantees that we include in the MODWT the whole internal wave frequency band, from fast gravity waves with typical period of $2\pi N^{-1}$ to the inertial motions (the inertial period at the latitude of the moorings is approximately 20 hours). Furthermore, this choice of time step guarantees that we separate the inertial and the semidiurnal lunar tidal motions (period 12.42 hours) in two different levels.

As an example, figure 3 shows the values of $\left\langle W^2 \right\rangle^M_{j,t}$ computed for the thermistor at the top of mooring 1. The results in the figure use $M = 101$, the value that is used throughout the paper. This value of M implies that the time series of $\left\langle W^2 \right\rangle^M_{j,t}$ has a time step of 707 s (we are working on a temperature time series low-pass filtered and subsampled to 7 s). This value is a compromise between higher statistical significance (higher M) and time resolution (lower M). Correlation between ϵ_{L_T} and ϵ_{L_E} (as well as L_T and L_E) weakly depends on the value M, with higher M giving slightly better correlation. However, a relatively small value of M is used in order to avoid reducing the observed range of values; averaging over longer time intervals removes the extreme values, and in particular leads to the undersampling of weakly turbulent phases. The figure clearly shows that most of the time series energy is concentrated in the low frequencies, which correspond to the semidiurnal tide and to the inertial frequencies. This gives further confidence that by low-pass filtering we neglect only a small part of the time series variance. The frequency band containing the semidiurnal tide frequency (second from below in the upper panel of figure 3) is particularly prominent, indicating that the dynamics are dominated by tides. It is also interesting to note that the energy is modulated at all frequencies, with particular strong variance at the beginning and end of the time series, most likely in connection with the passage of mesoscale or submesoscale features at the mooring location. Slow modulations are highly correlated among different bands, suggesting that larger scale motions have a strong impact on the internal wave activity at all frequencies.

Once the MODWT is available, the computation of L_E and ϵ_{L_E} is straightforward. Based on (5), L_E can be

computed as:

$$L_E = \frac{g\alpha}{N_\theta^2} \left(\Sigma_{J,t}^M\right)^{\frac{1}{2}}, \tag{11}$$

which expresses L_E as a function of the variance in the time series up to the level J of the MODWT. The value of J will be discussed in section III.

Similarly, combining (6) and (11), the variance-based estimate of the turbulence dissipation rate ϵ_{L_E} is computed as:

$$\epsilon_{L_E} = 0.64 \cdot \frac{N^3}{N_\theta^4} (g\alpha)^2 \Sigma_{J,t}^M. \tag{12}$$

Since L_T has been defined as a single value for the portion of the column measured by the thermistors (as the root mean square displacement, see I and II.C.1), equations (11) and (12) will be used only as a column mean, i.e. a function of time alone. The value of $\Sigma_{J,t}^M$ used in (11) and (12) is the vertical mean one. Furthermore, we assume that the physically relevant N is the vertical mean one, excluding from the mean the values computed at the top and bottom thermistors, where the estimation of the vertical derivative of temperature is less reliable. This is a more reasonable approach than considering only averages over single overturns, since the definition of an isolated overturn is rather arbitrary in the data set—overturns are often observed inside other overturns, and overturns can be only partially recorded in the dataset (the mooring does not cover the whole water column).

III. RESULTS

A. Mooring 1

1. Time scales

In the previous sections, the key point left unaddressed was the estimation of τ, i.e. the time scale over which the assumption of rigid advection of a mean temperature profile is valid (see section II.A). This point can now be addressed by evaluating the validity of (11) and (12) applied to the dataset of mooring 1. We measure the skill of our estimates by computing the cross-correlation between L_T and L_E (written in short $R[L_T, L_E]$), and between ϵ_{L_T} and ϵ_{L_E} (written in short $R[\epsilon_{L_T}, \epsilon_{L_E}]$). Table II collects the values of $R[L_T, L_E]$ and $R[\epsilon_{L_T}, \epsilon_{L_E}]$ computed for different levels J. We remind that the value of J determines the maximum period in the variance estimate $\Sigma_{J,t}^M$, entering equations (11) and (12). Table II shows that the correlation is high up to scale 7, i.e. periods of 30 min, and then quickly drops. It is interesting to note that this period roughly corresponds to $2\pi N_{99}^{-1}$ (20 min for mooring 1), which is a strong indication that the method works if most internal wave motions are removed from the data. Correlations lagged in time confirm that maximum correlation is attained for zero time lag (not shown). Based on this evidence, we conclude that τ is approximately 20 minutes. If, however, we use $J = 6$ or $J = 7$ for our estimates, we find that L_E systematically overestimates L_T with the only exception of the largest overturns (not shown). This is reminiscent of the results of Itsweire (1984), Itsweire *et al.* (1993) and Smyth and Moum (2000), and is probably linked to the inclusion of a significant part of the signal due to internal wave motions in the estimate. To overcome this problem, we will use the estimates with $J = 5$.

It is worthwhile to analyse more in detail the process leading to maximum correlation for short time scales, since this is one of the main results of the work. We want in particular to check if the loss of correlation for long time scales is really connected with the decorrelation of the mean temperature profile, which in our framework we assume is being rigidly advected by vertical motions. An alternative explanation may be connected to the typical duration of an overturning event. A water parcel is expected to return to its equilibrium position on a time of order N^{-1}, in particular $2\pi N^{-1}$ if gravity waves are generated; these are the time scales over which an overturning event may be expected to decay. On the other hand, horizontal advection at the mooring location may lead, on average, to an apparent faster return to equilibrium, by advecting the overturning patch away from the mooring. This latter hypothesis is not supported by the autocorrelation function of L_T, shown in figure 4-a. The figure shows the average correlation computed in linearly detrended subsets, lasting 4 days each, of the full time series of L_T from mooring 1. The inset in figure 4-a suggests that an overturning patch typically lasts approximately 1.7 hours (autocorrelation crossing the zero line); this closely corresponds to the time scale expected for gravity wave motions with N equal to the mean value at mooring 1. The correspondence between the decorrelation time of L_T and $2\pi N^{-1}$ may suggest that high-frequency internal waves near the buoyancy frequency play a major role in the decay of the overturns, but

it may also largely be due to chance. Further analysis of this interesting issue goes beyond the scope of this paper; the point to be made here is that the results seem not to be influenced by the advection of the patches. Time lags longer than one hour show anticorrelation, suggesting that an overturning event is more often followed by a quiescent period[3]. This is different from what was found by Alford and Pinkel (2000), who did not observe significant changes in Richardson number distribution before and after an overturn. This difference is probably to be attributed to the different measurement locations, here close to the bottom and strongly dominated by semidiurnal tide, while in Alford and Pinkel (2000) in the upper thermocline over relatively deep waters. Figure 4-a also shows that the semidiurnal tidal period of approximately 12.42 hour is clearly present in the L_T time series, confirming that the dynamics are to a large extent locked to the tide. Even if autocorrelation may be slightly overestimated due to the fact that we do not distinguish between overturns taking place at different depths, these features identified in the autocorrelation function of L_T give confidence that advection is not significantly disturbing our estimation procedure.

Further support for the hypothesis that τ is limited by changes in the vertical temperature profile comes from the autocorrelation function of temperature (figure 4-b). Autocorrelation of temperature is computed here from the two dimensional, time and depth dependent, temperature record and is lagged both in time and in depth. The use of a two-dimensional correlation function has the aim of identifying the decorrelation time of temperature with itself, taking into account the fact that vertical displacements can reduce the correlation computed at a fixed depth. However, since the time series is strongly self-correlated in particular due to the tidal signal, not relevant for the time scales considered here, the computation is performed on subsets of the complete time series of length approximately 4.8 hour, and linear detrending of the data set is performed both in time and depth. The results in figure 4-b clearly show that this detrended temperature profile is not correlated with itself after a few tens of minutes, and most of the correlation is lost already after 5 minutes. Correlation is maximum for zero depth lag (correlation for zero depth lag is reported in the inset), most likely due to the fact that we are looking at time scales faster than most of the waves in the system. The results from this brief study of the autocorrelation in the dataset thus support the conclusions drawn from Table II. In particular, we suggest that τ is limited by the loss of self-correlation of the temperature profile. This loss of self-correlation is likely due to the incoherent (turbulent) motions above the internal wave band, as suggested by considering the time scale $2\pi N_{99}^{-1}$ (approximately 20 min, drawn as a black dotted line in figure 4-b), which corresponds to an autocorrelation at zero depth lag of approximately 0.1. In practice, by using $J = 5$ in the MODWT we limit τ nominally to 7.5 min (black dashed line), corresponding to an autocorrelation of temperature at zero depth lag of 0.4. We remember, however, that spectral leakage will lead, to some extent, to the inclusion also of longer periods.

2. Length scales and turbulence dissipation rate

Figure 5-a shows L_E computed using equation (11) as a function of L_T. In equation (11) we used $J = 5$ and $M = 101$ as discussed in section II.C.2. In general, we find that L_E based on the MODWT provides on average a good estimate of L_T computed by reordering the temperature profile. Medians of the estimates are shown as red triangles in the figure, computed by binning the results in 14 classes, equally spaced in the $\log_{10}(L_T)$ space. The dispersion of the estimates is less than a factor of 2 (0.3 in the logarithmic space of the plot), as measured by their standard deviation (red error bars in the figure). L_E underestimates, on average, L_T at large values. This has to be expected since (11) is based on a linear approximation, breaking down for larger values of the displacement. On the other hand, there is a slight overestimation of L_T by L_E for smaller overturns, substantially less evident than in Itsweire (1984) and Smyth and Moum (2000). Overall, the relationship between L_E and L_T is less than linear. This fact, already observed in the DNS simulations of Smyth and Moum (2000), is probably due to a combination of residual internal wave signal and to the non uniformity of the temperature gradient. Estimates of L_E including internal wave motions have too low correlation with L_T to distinguish a stronger overestimation of L_T for smaller overturns. Finally, we note that the length of mooring 1 imposes a cutoff for large L_T, already shown in figure 2-a, which is not affecting the MODWT-based estimates of L_E.

Very similar conclusions can be drawn from figure 5-b, which shows ϵ_{L_E} as a function of ϵ_{L_T}. Correlation is in this case lower, but the method based on the MODWT still provides, on average, a good estimate of ϵ_{L_T}. The spread between the two quantities is also in this case larger for larger values, but the effect of the large scale cutoff in L_T is not obvious as in panel a, since N is included in the computation. However, it is very likely that a significant number of the largest ϵ_{L_T} values is underestimated due to the cutoff in L_T.

---

[3] The autocorrelation is always computed on a time series whose mean has been removed. A negative autocorrelation obviously does not imply a negative L_T, only an L_T smaller than the mean value.

B. Moorings 2 and 3

The analysis described for mooring 1 was applied to moorings 2 and 3. In this case, the lower values of N lead to the use of a higher J. In particular, given that $2\pi N_{99}^{-1} \approx 30$ min, we use $J = 6$, i.e. we include periods nominally up to 15 min. As discussed for mooring 1, since spectral leakage is unavoidable, this represents a conservative choice which provides good results. The results are shown in figure 6, respectively panels a and b for mooring 2 and panels c and d for mooring 3. The same procedure applied to these two data sets leads to lower correlation between L_T and L_E and between ϵ_{L_T} and ϵ_{L_E} compared to mooring 1. The reasons for the worse agreement are the broader distribution of N (which makes the linear approximation worse) and the lower signal to noise ratio in these data sets as compared to the one from mooring 1. Panels a and c in figure 6 clearly show that the largest L_T's are well resolved, mostly due to the presence of few large overturns rather than due to the use of longer moorings. This is clear also from panels b and d, which show that the highest values of turbulence dissipation rate in moorings 2 and 3 are at least an order of magnitude smaller than in mooring 1.

Despite these differences, the results from mooring 1 are confirmed. There is clear correlation between the quantities computed by reordering the temperature profile, and those computed by analysing the variance in the temperature time series at a fixed depth. Moorings 2 and 3 show that L_E and ϵ_{L_E} systematically underestimate their Thorpe-scale-based counterparts for the largest events, a fact that was not clear from mooring 1 due to the cutoff of large overturns therein. The Thorpe scale is in fact underestimated by L_E also for smaller values in mooring 2. Above $\epsilon_{L_T} \approx 10^{-7}$ m^2 s^{-3}, the L_E-based estimates seem to saturate, even if the high dispersion and the relatively few samples prevent a clearer identification of the change in behaviour.

This underestimation and less-than-linear relationship is most likely a combined effect of the broader N distribution and of the filtering procedure applied here. In particular, by considering variance only in a portion of the frequency spectrum, we neglect the overturns associated with longer time scales (i.e. the ones whose dynamics are linked to weaker stratification). As discussed above, the J-level we use is a conservative choice, which can lead to underestimation of the Thorpe scales counterparts. The spectral leakage makes it difficult to strictly control the frequency band actually included in the analysis; the cutoff frequency is thus always approximate, and, in our view, a conservative approach has to be preferred for this reason. The filtering procedure is, in any case, essential to have a high correlation between the different estimates, as discussed with Table II.

IV. DISCUSSION

The results presented in the previous sections demonstrate that the analysis of temperature variance is a viable alternative to Thorpe scales analysis when sufficiently high time resolution is available. In the best case scenario, which is represented here by mooring 1, the results from the MODWT can provide a quantitative estimate of L_T and of ϵ_{L_T} over a wide range of values, on average approximately within a factor of 2. Even for more challenging data sets, however, as those recorded at moorings 2 and 3 (lower signal-to-noise-ratio, larger spread and lower values of N), the analysis technique described here can provide valuable information. Furthermore, the technique can reliably distinguish phases with stronger turbulence from phases with weaker one at a mooring location, even when the quantitative agreement is lost (e.g. strongest turbulence dissipation rate in moorings 2 and 3).

It must be stressed here that the correlation between ϵ_{L_E} and ϵ_{L_T} is for the largest part due to the correlation between the temperature variance and the displacement. In other words, correlation between ϵ_{L_E} and ϵ_{L_T} is not a consequence of using the same N in the computation of the two estimates. In fact, N is only weakly correlated (order of 0.1) with ϵ_{L_T}, while $\Sigma_{J,t}^M$ has a much higher correlation with ϵ_{L_T} (order of 0.6). Only if the average over the whole time series at each depth is considered separately, N is correlated with the turbulence dissipation rate, as deeper portions of the water column, closer to the bottom boundary layer, experience on average weaker stratification and stronger turbulence (as discussed for instance in Alford and Pinkel, 2000, their figure 25).

If we want to identify the sources of error in (5), we can consider the propagation of the error in temperature according to the formula:

$$\frac{\varepsilon_{L_E}}{L_E} \approx \frac{\varepsilon_{\theta_{\hat{z}}}}{\theta_{\hat{z}}} + \frac{3g\alpha}{\Delta z}\frac{\varepsilon_{\theta_{\hat{z}}}}{N_\theta^2}, \tag{13}$$

where ε_x represents the absolute error of x, Δz is the vertical sensor distance, whose small error is neglected, and the factor 3 comes from the use of centred derivatives. Considering the sensor noise as the largest source of error, a signal-to-noise ratio (for temperature) better than 10^2 (for the high frequency variations) should be sufficient to have a precise estimation of L_E if only the first term on the right hand side of (13) is taken into account. Considering

figure 3, we see that at mooring 1, typical variations of temperature at periods shorter than 15 min are of the order of $10^{-2\circ}$ C (as confirmed by considering the MODWT decomposition of the whole data set; note that figure 3 shows the variance rather than to the root mean square of the time series). The signal-to-noise ratio is thus well above 10^2 in mooring 1, having a typical noise level of $5 \cdot 10^{-5\circ}$ C. The other two moorings represent a less optimal case, mainly due to the smaller temperature variations, closer to $10^{-3\circ}$ C in the frequency range considered. Using mean values from the data considered in this work, the second term on the right hand side of (13) is the main contribution to the relative error, being in the order of 10%. The relative error grows as N_θ^{-2} for weak stratification, and estimates with weaker stratification are thus more affected, and this is one of the reason for the worse correlation observed for moorings 2 and 3. However, in view of this error analysis which does not explain the observed dispersion, we suggest that the main source of error in the results is in fact the linear approximation of (2). This is unsurprising, since we are linearly approximating a signal which is generated by a highly non-linear process, i.e. the overturning of a stratified fluid.

The skill of our estimates is particularly interesting if sufficiently long time series are available, from which the correlation between mesoscale dynamics and turbulence can be inferred, a subject that we aim to explore in detail in the future. On the other hand, the results presented here leave open the issue of the accuracy of the estimates in comparison to direct measurements from microstructure profilers. This comparison, unavailable for the datasets discussed here, would be particularly interesting considering that ϵ_{L_T} is likely overestimating the real turbulence dissipation rate during the initial phase of the turbulence evolution and possibly underestimating it during the late stage of turbulence decay, as suggested by the numerical simulations of Smyth and Moum (2000) and Mater *et al.* (2013). If this is true, it may be worth considering ϵ_{L_E} for estimating turbulence dissipation rate in these phases.

Furthermore, the method described here may have an important practical application. If only temperature measurements are available, a non-tight temperature-salinity relationship may produce inversions in the temperature profile which do not correspond to a density inversion. By estimating the overturns length scale through Eulerian measurements, i.e. measurements at a fixed depth, this method may provide an alternative to Thorpe scales estimation if sufficient temporal resolution is available. Using a value of N from, e.g., climatological data, the turbulence dissipation rate, or at least its variations in time with respect to a reference level, may be measured. This is particularly interesting considering the high correlation between the temperature variance and ϵ_{L_T} mentioned above.

Finally, it is worth discussing the link between our results and the classical problem of fine structure contamination. As noted already by Phillips (1971), the measurement of vertical displacement spectra from Eulerian measurements of temperature in layered media is hindered by the power leakage towards the high frequency portion of the spectrum. This problem, well known in the literature, is believed to render the high frequency end of the temperature spectra mostly unusable (Garrett and Munk, 1971; Gostiaux and van Haren, 2012; McKean, 1974; Siedler, 1974). There is no doubt about the fact that fine structure contamination is present in the datasets presented here, since layering is obvious in the temperature profiles. However, the results show that there still is precious information available in the high frequency part of the temperature spectrum, despite fine structure contamination. Gostiaux and van Haren (2012) demonstrated that the amount of power leaked from the internal wave band to higher frequencies increases with more abrupt steps in the advected profile. This suggests that higher values of ϵ_{L_E} should be associated with more abrupt steps too. In order to check this hypothesis, we plot in figure 7 ϵ_{L_E} as a function of the variance of N, computed at each time step from the quadratically detrended vertical profile of N. The variance of N is the simplest measure of the layering we can define from the temperature profile. The data in figure 7 is strongly scattered, but there is a clear hint of positive correlation between these two quantities, in particular for higher values of σ_N^2 and ϵ_{L_E}. The reasons for the strong scatter in figure 7 are manifold. Our measure of the steppiness, i.e. the variance of N, does not distinguish between sharp steps and variations not captured by the quadratic detrending; a more careful analysis of the variance of N is possible, but goes beyond the scope of the present paper. Furthermore, for smaller values of ϵ_{L_E}, i.e. smaller L_E, the variance estimate used in the figure may not be the correct one, since the variance is computed here over the whole column (which smaller overturns do not sample in its entirety). Finally, scatter is caused by the break down of the hypothesis of rigid advection of the vertical profile. Despite all these limitations, we suggest that stronger turbulence may be associated with stronger layering in the water column, even if we are unable to disentangle cause from effect using the results of this work.

V. SUMMARY

We discussed different ways of estimating overturning length scales from records of temperature. We outlined a method for estimating the scales of overturns using frequency spectra of temperature beyond the internal wave band, using Eluerian measurements from moored thermistors. We presented three recent oceanographic data sets of

temperature, recorded close to the bottom at different slopes of Seamount Josephine (North Eastern Atlantic Ocean). We found clear correlation between Thorpe and Ellison scales in these observations, similarly to previous numerical and laboratory experiments. We pointed out the importance of a time–frequency decomposition of variance in order to find a good correlation between Thorpe and Ellison scales in oceanographic data sets. In particular, we observed the highest correlation when frequencies beyond the internal wave band are considered, and we linked this to the loss of autocorrelation of the vertical temperature profile, probably due to diabatic process. Finally, we discussed how these results suggest a possible use for records that suffer from fine structure contamination, and how this is linked to the layering of the column.

The authors would like to thank the crew of RV Pelagia for enabling the deployment and recovery of the instruments, and all the technicians, in particular Martin Laan, indispensable for the success of the measurements.

REFERENCES

Alford, M. H., and R. Pinkel (2000), Journal of Physical Oceanography **30** (5), 805.
Cornish, C. R., C. S. Bretherton, and D. B. Percival (2006), Boundary-Layer Meteorology **119** (2), 339.
Crawford, W. R. (1986), Journal of Physical Oceanography **16** (11), 1847.
Dillon, T. M. (1982), Journal of Geophysical Research: Oceans **87** (C12), 9601.
Ebisuzaki, W. (1997), Journal of Climate **10** (9), 2147.
Frisch, U. (1996), *Turbulence* (Cambridge University Press, Cambridge, U.K.).
Gargett, A. E. (1988), Journal of Geophysical Research: Oceans **93** (C5), 5021.
Gargett, A. E. (1989), Annual Review of Fluid Mechanics **21** (1), 419.
Garrett, C., and W. Munk (1971), Journal of Physical Oceanography **1** (3), 196.
Gostiaux, L., and H. van Haren (2012), Journal of Geophysical Research: Oceans **117** (C11), C11003.
Gregg, M. C. (1987), Journal of Geophysical Research: Oceans **92** (C5), 5249.
Hans van Haren,, M. Laan, D.-J. Buijsman, L. Gostiaux, M. Smit, and E. Keijzer (2009), IEEE Journal of Oceanic Engineering **34** (3), 315.
van Haren, H., and L. Gostiaux (2009), Journal of Geophysical Research: Oceans **114** (C5), C05005.
van Haren, H., and L. Gostiaux (2011), Geophysical Research Letters **38** (22), L22603.
van Haren, H., and L. Gostiaux (2012), Journal of Marine Research **70** (1), 173.
van Haren, H., L. Gostiaux, M. Laan, M. van Haren, E. van Haren, and L. J. A. Gerringa (2012), PLoS ONE **7** (3), e32535.
Itsweire, E. C. (1984), Physics of Fluids **27** (4), 764.
Itsweire, E. C., J. R. Koseff, D. A. Briggs, and J. H. Ferziger (1993), Journal of Physical Oceanography **23** (7), 1508.
Jones, E., T. Oliphant, P. Peterson, *et al.* (2001), "SciPy: open source scientific tools for python, www.scipy.org," .
Lueck, R. G., F. Wolk, and H. Yamazaki (2002), Journal of Oceanography **58** (1), 153.
Mater, B. D., S. M. Schaad, and S. K. Venayagamoorthy (2013), Physics of Fluids **25** (7), 076604.
McKean, R. S. (1974), Journal of Physical Oceanography **4** (2), 200.
Oakey, N. S. (1982), Journal of Physical Oceanography **12** (3), 256.
Percival, D. B., and A. T. Walden (2006), *Wavelet Methods for Time Series Analysis* (Cambridge University Press, Cambridge, U.K.).
Phillips, O. M. (1971), Journal of Physical Oceanography **1** (1), 1.
Polzin, K. L., J. M. Toole, J. R. Ledwell, and R. W. Schmitt (1997), Science **276** (5309), 93, PMID: 9082993.
Siedler, G. (1974), Deep Sea Research and Oceanographic Abstracts **21** (1), 37.
Smyth, W. D., and J. N. Moum (2000), Physics of Fluids **12** (6), 1327.
Smyth, W. D., J. N. Moum, and D. R. Caldwell (2001), Journal of Physical Oceanography **31** (8), 1969.
Thorpe, S. A. (1977), Royal Society of London Philosophical Transactions Series A **286**, 125.
Torrence, C., and G. P. Compo (1998), Bulletin of the American Meteorological Society **79** (1), 61.

Mooring number	1	2	3
Latitude	36 58.885 N	37 01.431 N	37 01.237 N
Longitude	13 45.523 W	13 39.479 W	13 39.367 W
Deepest thermistor	2210 m	2937 m	2937 m
Height above bottom	5 m	5 m	5 m
Number of thermistors	144	140	170
Thermistor spacing	0.7 m	1.0 m	1.0 m
Length	100.1 m	139 m	169 m
Deployment	13 Apr 2013	12 Aug 2013	12 Aug 2013
Recovery	12 Aug 2013	18 Oct 2013	18 Oct 2013

Table I Details of the three data sets from three different moorings used in the paper. The length reported is the length over which thermistors are actually attached to.

J	Max. period	$R[L_T, L_E]$	$R[\epsilon_{L_T}, \epsilon_{L_E}]$
1	28 s	0.78	0.68
2	56 s	0.79	0.69
3	1.9 min	0.80	0.70
4	3.7 min	0.80	0.71
5	7.5 min	0.81	0.71
6	15 min	0.80	0.70
7	30 min	0.79	0.67
8	60 min	0.75	0.62
9	2 hour	0.69	0.52
10	4 hour	0.62	0.42
11	8 hour	0.58	0.36
12	16 hour	0.53	0.31
13	32 hour	0.54	0.30

Table II Cross-correlation between L_T and L_E, and between ϵ_{L_T} and ϵ_{L_E}. The J reported in the first column is the maximum level used for computing $\Sigma^M_{J,t}$ in (11) and (12). The second column reports the maximum period nominally included in $\Sigma^M_{J,t}$. In all cases, $M = 101$. Taking into account the autocorrelation of the time series with the method of Ebisuzaki (1997), all the values of cross-correlation reported are above the 99% significance level, thanks to the length of the time series.

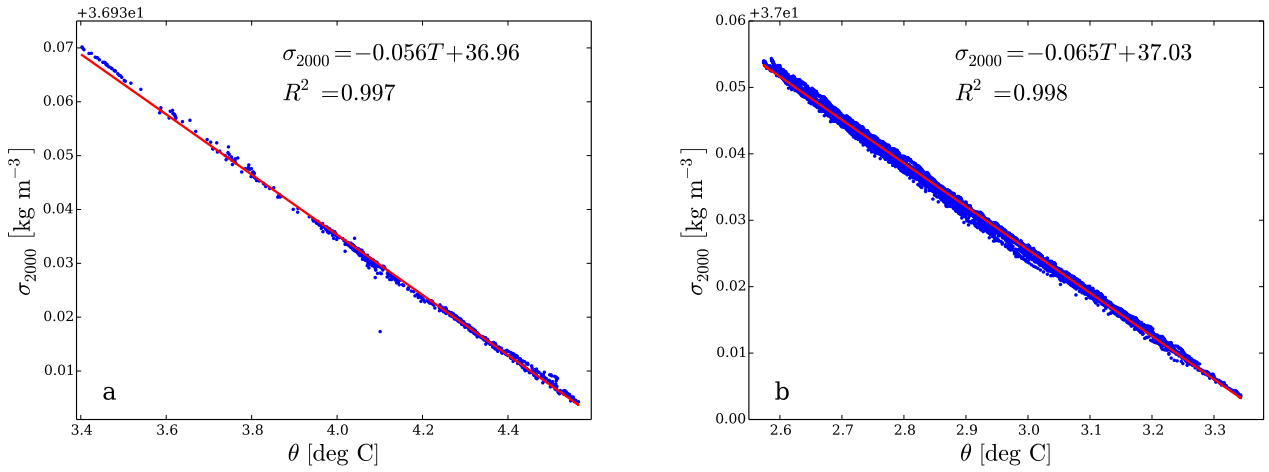

Figure 1 Summary of the two CTD surveys performed (see text), showing in each panel the density–temperature relation for data between 2000 m and 2500 m in panel a, between 2000 m and 3000 m in panel b. Data are 2 m bin averages from downward CTD casts. The results of a linear fit of the data are shown in the two panels.

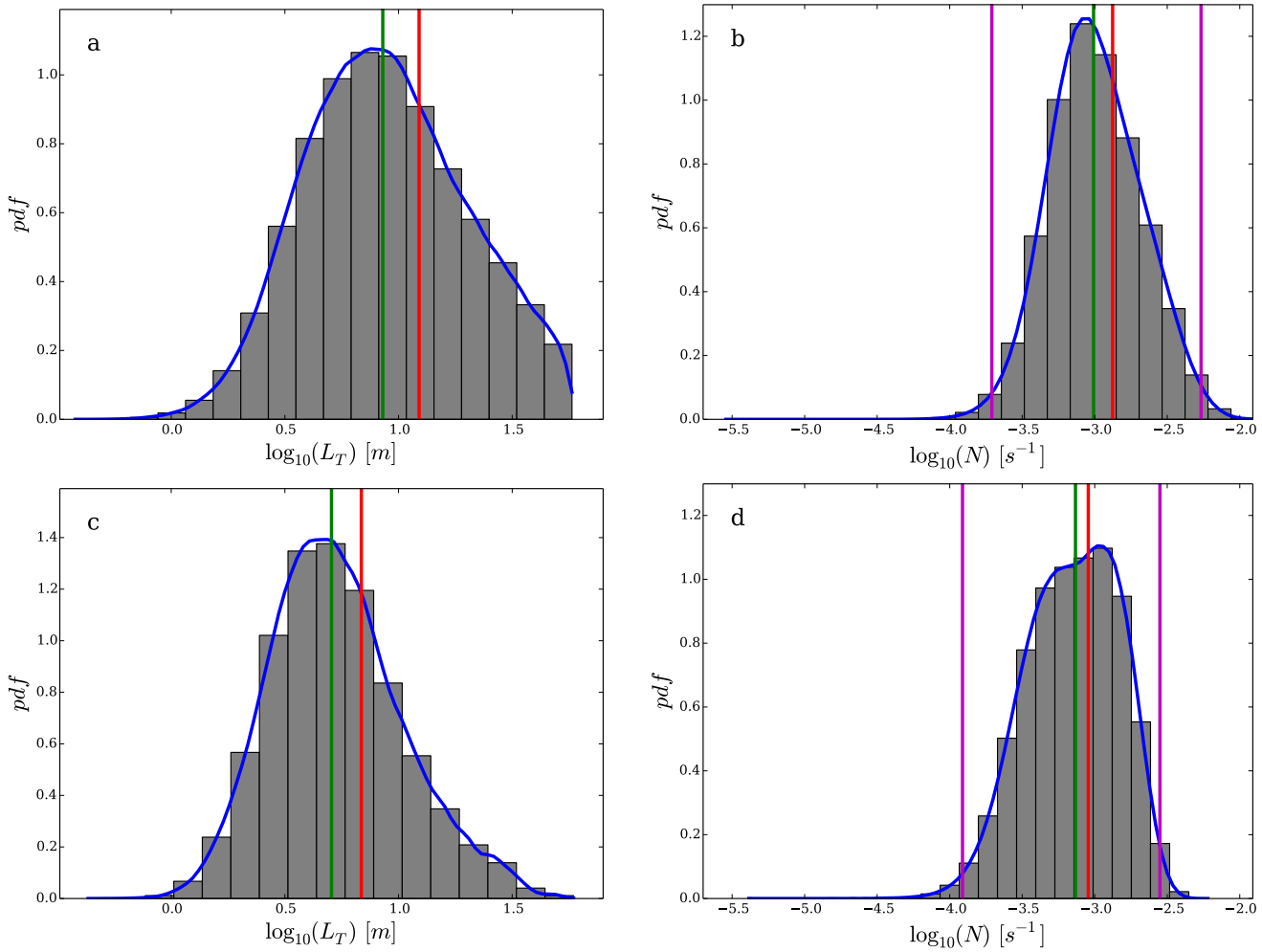

Figure 2 Probability density function of the logarithm of the Thorpe scale (mooring 1: panel a, mooring 2: panel c) and of the logarithm of the buoyancy frequency (mooring 1: panel b, mooring 2: panel c), as obtained by binning the data (grey bars) and by using a Gaussian kernel estimator (blue line, see Jones *et al.*, 2001, for details). The mean (vertical red line) and median (vertical green line) of the ensemble are also shown. In panels b and d, the pink lines mark N_1 and N_{99}. Results for mooring 3 (not shown) are mostly equivalent to those of mooring 2.

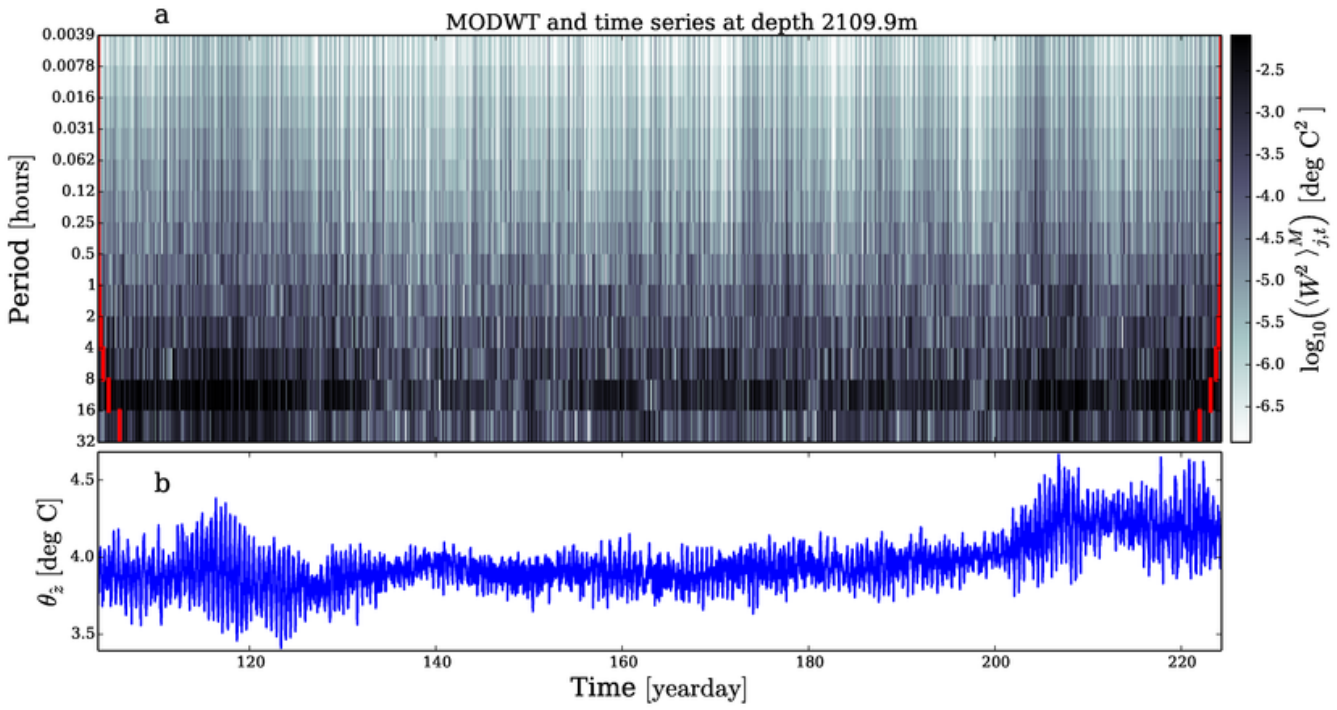

Figure 3 Panel a: results for MODWT from a single thermistor at the top of mooring 1 (depth 2109.9 m). The running mean of wavelet variance is shown, $\langle W^2 \rangle_{j,t}^M$, as a function of time and period. The results are from a "least asymmetric" wavelet filter of length 8, and use $M = 101$. The vertical red lines mark the coefficient furthest away from each boundary which is influenced by boundary conditions (i.e. computed using values outside the original time series, see text). The log colour scale saturates at the 2nd and 98th percentiles. Panel b: time series of temperature used in the MODWT shown in panel a. The time axis has units of yeardays, i.e. 1 January 2013 12:00UTC is yearday 0.5.

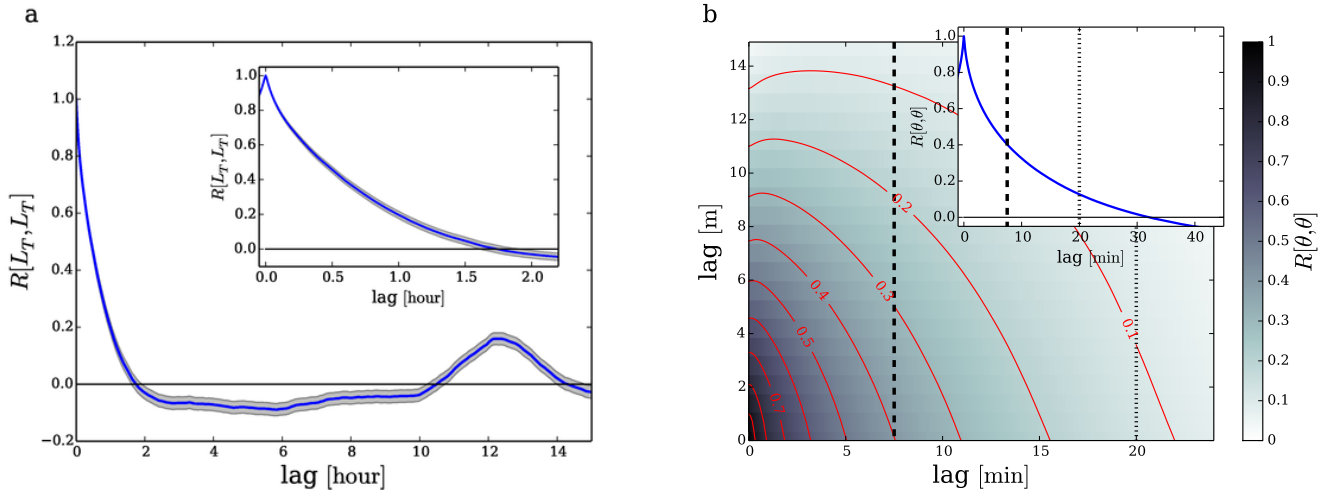

Figure 4 Autocorrelation function of Thorpe scale (panel a) and temperature (panel b) at mooring 1. Panel a shows correlation lagged in time, with the detail close to zero lag in the inset. The grey shaded area marks the 99% confidence interval of the correlation. Panel b shows correlation lagged both in time (horizontal) and in depth (vertical), computed from the two dimensional, time–depth dependent, temperature field. In the inset of panel b, the autocorrelation for zero depth lag is reported. The red contours mark correlation values of 0.1, 0.2, 0.3, 0.4, 0.5, 0.6, 0.7, 0.8, 0.9. The black vertical lines mark the maximum period nominally included in the estimates from MODWT (dashed) and $2\pi N_{99}^{-1}$ (dotted); see text for details.

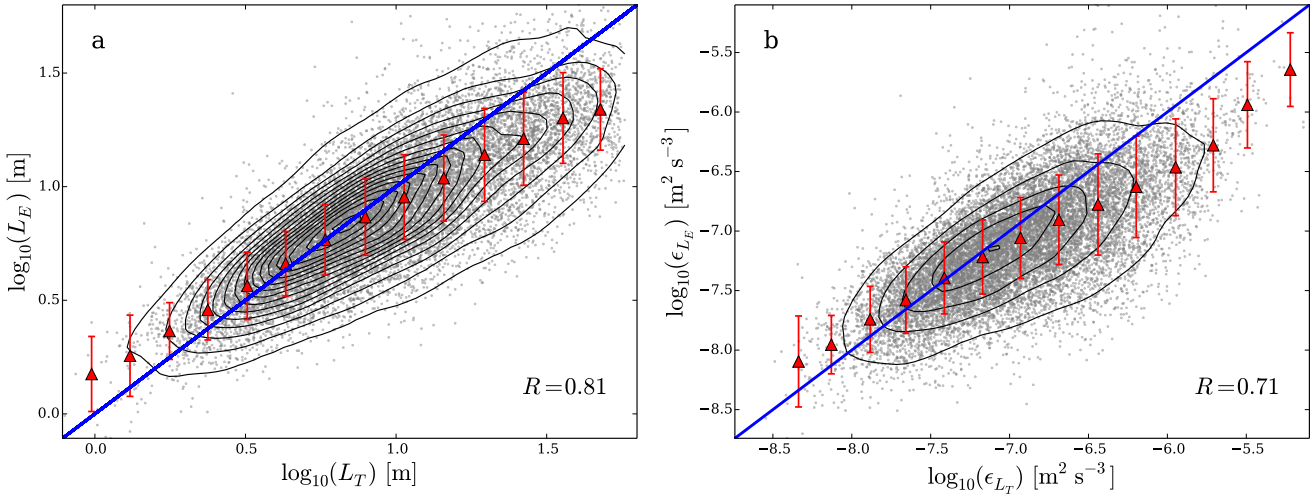

Figure 5 Results from mooring 1, using $J = 5$ (longest nominal period 7.5 min). Panel a: L_E as a function of L_T. Each grey dot is an estimate based on running averages over 707 s (see text). The black contours show the probability density function of the results, estimated with a Gaussian kernel (Jones *et al.*, 2001); the contours mark the values of the probability density function at intervals of 0.1 starting from 0.1. The blue line marks $L_E = L_T$. The red triangles mark the median of the distribution of points, computed in 14 bins; the error bars are the standard deviation of the distribution. Correlation between L_T and L_E is reported from Table II. Panel b: same as panel a but for ϵ_{L_E} and ϵ_{L_T}.

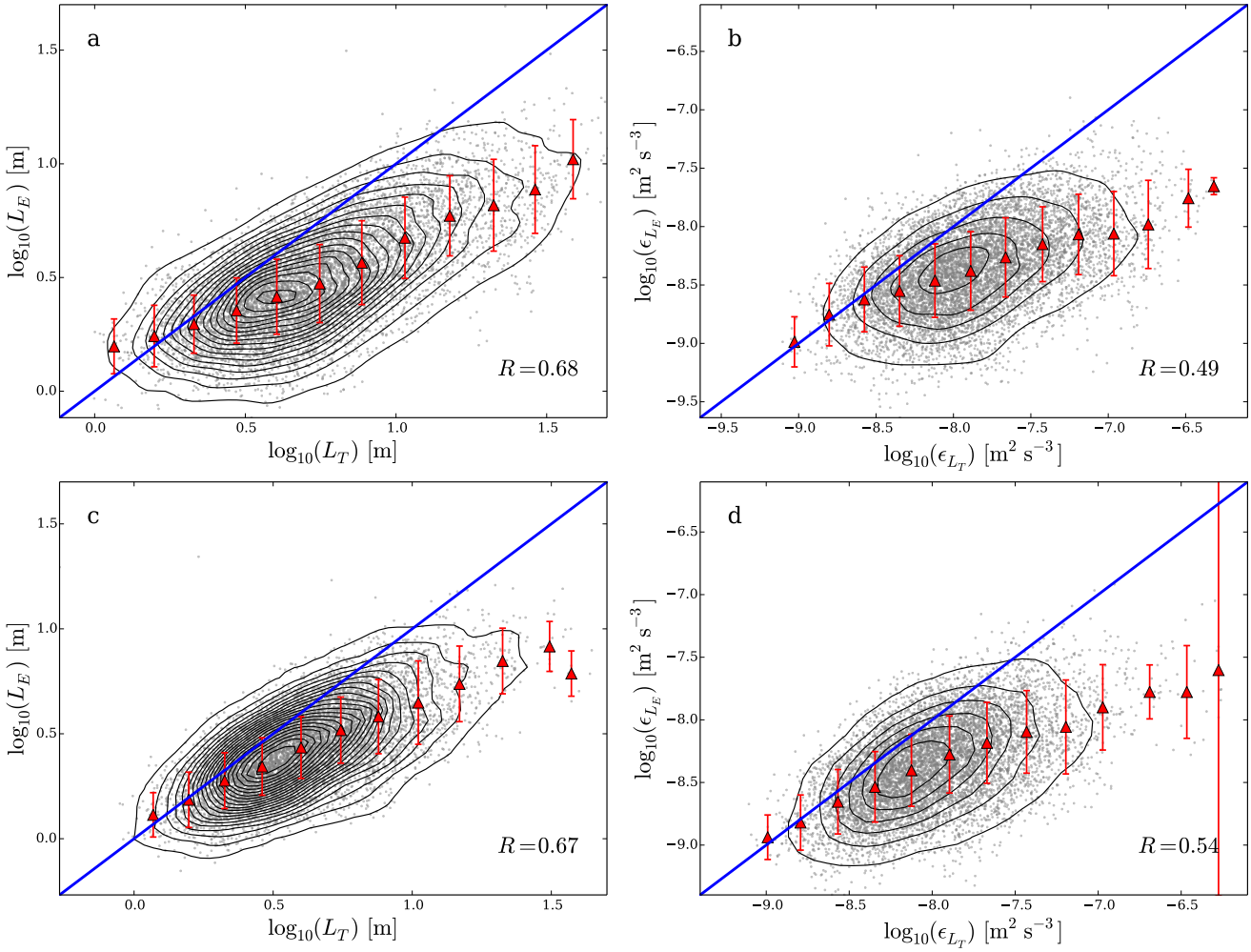

Figure 6 Same as figure 5 for moorings 2 (panels a and b) and 3 (panels c and d). For these two moorings, $J = 6$ was used (longest nominal period 15 min, see text).

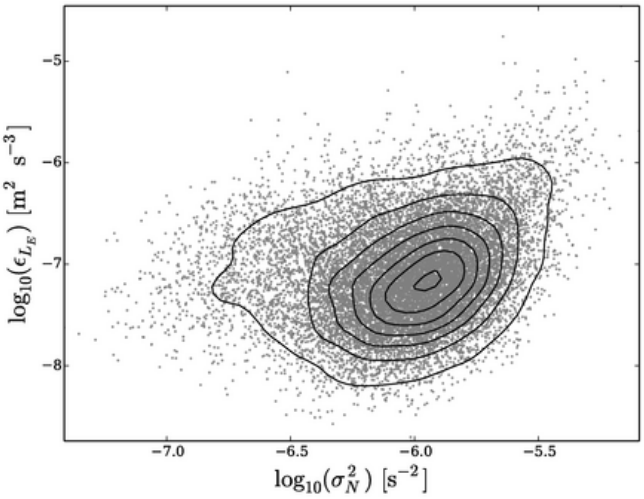

Figure 7 Turbulence dissipation rate estimated from MODWT (ϵ_{L_E}), as a function of the variance of N, computed at each time step from the quadratically detrended vertical profile of N. The black contours show the probability density function of the results, estimated with a Gaussian kernel (Jones *et al.*, 2001); the contours mark the values of the probability density function at intervals of 0.1 starting from 0.1.